JOURNAL OF COMPUTATIONAL PHYSICS **138,** 171–192 (1997)
ARTICLE NO. CP975818

A New Scheme to Treat the Numerical Tcherenkov Instability for Electromagnetic Particle Simulations

F. Assous,* P. Degond,† and J. Segré*

**CEA/LV, 94195 Villeneuve-St-Georges, France; †MIP, UFR MIG, UPS, 31062 Toulouse Cedex, France*
E-mail: assous@limeil.cea.fr

Received December 6, 1996; revised July 25, 1997

The aim of this paper is to present a new explicit time scheme for electromagnetic particle simulations. The main property of this new scheme, which depends on a parameter, is to reduce and in some cases to suppress numerical instabilities that can appear in this context and are widely described in the literature. Other numerical properties are also investigated, and a numerical example is finally given to illustrate our purpose. © 1997 Academic Press

Key Words: Vlasov–Maxwell system; numerical Tcherenkov; dispersion relation; pic code; plasma instability.

1. INTRODUCTION

The numerical simulation of charged particle beams or plasma physics phenomena requires methods of solution for the time-dependent coupled Maxwell–Vlasov system. In this framework, various authors have pointed out some specific problems such as unphysical noises and instabilities which may appear when particle simulations are coupled with grid methods such as finite differences or finite elements [1–3]. Theoretical studies have predicted these instabilities will arise [1, 4], and numerical experiments have confirmed their existence [5].

The interpretation of such instabilities is based on analysis of the numerical dispersion relation [6, 7], that is a relation between each wavenumber k and a propagation velocity v_ϕ (the phase velocity) which is an approximation of the light velocity c. When v_ϕ falls below c, an instability can be produced by an unphysical resonance between the electromagnetic waves propagating at v_ϕ and particles that are moving faster. For this reason, Godfrey [8] refers to this effect as a numerical Tcherenkov instability.

0021-9991/97 $25.00

The principle of the study consists in linearizing the system of equations and applying a Fourier transform in space and time to obtain a description of perturbations as a superposition of harmonics of the form $\exp \imath(kx - \omega t)$. One obtains a condition relating ω and k called the dispersion relation. If the roots $\omega(k)$ of this relation are complex, an instability can appear because complex roots usually appear in complex conjugate pairs. However, the linearization and the Fourier transform are theoretically valid under some regularity assumptions (uniform plasmas or sufficiently smooth data). Nevertheless, the results obtained are commonly extended outside these assumptions (in particular for stiff beams), according to the practice.

Several approaches were proposed to find remedies for this instability. High-order finite difference methods in the same spirit as in [9], implicit time schemes, or finer resolutions can be used, since they improve the dispersion relations. They are, however, not convenient to use because of difficulty in implementation. Other options have been presented and are essentially based on temporal and spatial filtering techniques [10–13].

In this article, we propose a new scheme to discretize the Maxwell equations that reduces, and in some cases suppresses, the numerical instability, according to the value of a parameter ε. Section 2 is devoted to a presentation of the scheme in terms of finite differences and finite element methods. Some elementary numerical properties, useful for a numerical implementation, are proved. The dispersion relation is derived from the relativistic fluid plasma linear analysis in Section 3, where the behavior of this new scheme with regard to instabilities is also investigated. These results are supported by a numerical example given in Section 4. Finally, a conclusion is drawn in Section 5.

2. PRESENTATION OF THE NEW SCHEME

2.1. The Vlasov–Maxwell Problem

2.1.1. *The Continuous Problem*

We consider a population of charged particles with a mass m and a charge q. The motion of these charged particles can be described in terms of particle distribution functions by the relativistic Vlasov equation,

$$\frac{\partial f}{\partial t} + V \cdot \frac{\partial f}{\partial X} + \mathscr{F} \cdot \frac{\partial f}{\partial P} = 0, \tag{2.1}$$

where $f(X, P, t)$ denotes the distribution function, $V = V(P)$ is the velocity, and $\mathscr{F} = \mathscr{F}(X, P, t)$ is the electromagnetic force, with the relations:

$$P = \gamma m V,$$
$$\gamma m = \frac{\sqrt{|P|^2 + m^2 c^2}}{c},$$

and

$$\mathscr{F} = q(E + V \times B). \tag{2.2}$$

In (2.2), $E = E(X, t)$ and $B = B(X, t)$ are the electric and magnetic fields which are solutions of the vacuum Maxwell equations:

$$\frac{\partial E}{\partial t} - c^2 \nabla \times B = -\frac{1}{\varepsilon_0} J, \tag{2.3}$$

$$\frac{\partial B}{\partial t} + \nabla \times E = 0, \tag{2.4}$$

$$\nabla \cdot E = \frac{\rho}{\varepsilon_0}, \tag{2.5}$$

$$\nabla \cdot B = 0. \tag{2.6}$$

The charge and current densities ρ and J are obtained from the solution f of the Vlasov equation according to

$$\rho = q \int_{\mathbb{R}^3} f \, dp, \quad J = q \int_{\mathbb{R}^3} V(p) f \, dp. \tag{2.7}$$

As we previously presented in [14], we rewrite Eqs. (2.3) and (2.4) in terms of two second-order wave equations (by using the identity $\nabla \times (\nabla \times U) - \nabla(\nabla \cdot U) = -\Delta U$), so that E is a solution of

$$\frac{\partial^2 E}{\partial t^2} - c^2 \Delta E = -\frac{1}{\varepsilon_0} \frac{\partial J}{\partial t} - \frac{c^2}{\varepsilon_0} \nabla \rho, \tag{2.8}$$

$$\nabla \cdot E = \frac{1}{\varepsilon_0} \rho, \tag{2.9}$$

and B is a solution of

$$\frac{\partial^2 B}{\partial t^2} - c^2 \Delta B = \frac{1}{\varepsilon_0} \nabla \times J, \tag{2.10}$$

$$\nabla \cdot B = 0. \tag{2.11}$$

It makes sense now to study a 1D discretization of the system (2.8)–(2.10) while it was not possible for the initial system (2.3)–(2.4).

We supplement this system with appropriate boundary and initial conditions. The boundary conditions may be perfectly conducting conditions, absorbing conditions, or symmetry conditions. We refer again to [14], where the issue of the well-posedness of the second-order wave equations in connection with the choice of boundary and initial conditions has been thoroughly discussed.

2.1.2. *The Discretization*

The Vlasov equation is numerically solved by means of a particle method. The distribution function $f(\cdot, \cdot, t)$ is approximated at any time t, by a linear combination of delta distributions in the phase space,

$$f(X, P, t) = \sum_k w_k \, \delta(X - X_k(t))\delta(P - P_k(t)), \tag{2.12}$$

where each term of the sum can be identified with a macro-particle, characterized by its weight w_k, its position X_k, and its momentum P_k. This distribution function is a solution of the Vlasov equation (2.1) if and only if (X_k, P_k) is a solution of the differential system:

$$\frac{dX_k}{dt} = V_k = \frac{P_k}{\gamma_k m}, \tag{2.13}$$

$$\frac{dP_k}{dt} = \mathscr{F}(X_k, P_k), \tag{2.14}$$

which describes the time evolution of a particle k, submitted to the electromagnetic force $\mathscr{F}$. This system is numerically solved by a leapfrog scheme (see [15] for more details).

We now recall the finite element formulation we used in [14]. Since the two wave equations (2.8) and (2.10) are of the same mathematical nature, we will concentrate on one of them, namely the E-wave equation (2.8). The variational formulation associated with (2.8) is written, in the case of perfect conductor boundary conditions:

$$\frac{d^2}{dt^2}\int_\Omega E \cdot F \, dx + c^2 \int_\Omega \nabla E : \nabla F \, dx = -\frac{1}{\varepsilon_0}\frac{d}{dt}\int_\Omega J \cdot F \, dx + \frac{c^2}{\varepsilon_0}\int_\Omega \rho \nabla \cdot F \, dx \quad \forall F, \tag{2.15}$$

where F is a test function chosen in an appropriate functional space. The reader may refer to [14] for more details on the mathematical background of this formulation. If we define suitable approximations spaces (in the following, it will be always the $P1$ nodal element, namely continuous functions with their restriction to each element being a polynomial of degree 1) and apply the leapfrog scheme in time, we obtain the following time discretization:

At each time step find the E_h^{n+1} solution of

$$\begin{aligned} &\frac{1}{\Delta t^2}\int_\Omega (E_h^{n+1} - 2E_h^n + E_h^{n-1}) \cdot F_h \, dx + c^2 \int_\Omega \nabla E_h^n \cdot \nabla F_h \, dx \\ &\quad = -\frac{1}{\varepsilon_0}\frac{1}{\Delta t}\int_\Omega (J_h^{n+1/2} - J_h^{n-1/2}) \cdot F_h \, dx + \frac{c^2}{\varepsilon_0}\int_\Omega \rho_h^n \nabla \cdot F_h \, dx \quad \forall F_h. \end{aligned} \tag{2.16}$$

We denote by $[E_h]$ the column vector made of the degrees of freedom of E_h and $[F_h]^t$ the row vector made of the degrees of freedom of F_h. We then introduce the mass matrix, the rigidity matrix, and the "gradient matrix," respectively defined by

$$[F_h]^t M[E_h] = \int_\Omega E_h \cdot F_h \, dx, \quad [F_h]^t K[E_h] = \int_\Omega \nabla E_h \cdot \nabla F_h \, dx, \quad [F_h]^t L\rho = \int_\Omega \rho_h \nabla \cdot F_h \, dx, \tag{2.17}$$

so that (2.16) is written as (we drop the subscript h and the [ ]):

At each time step find the E^{n+1} solution of

$$\frac{1}{\Delta t^2} M(E^{n+1} - 2E^n + E^{n-1}) + c^2 K E^n = -\frac{1}{\varepsilon_0} M(J^{n+1/2} - J^{n-1/2}) + \frac{c^2}{\varepsilon_0} L\rho^n. \tag{2.18}$$

As the mass matrix is not diagonal, we have to invert at each time step a linear system the dimension of which is the dimension of the finite element space. In order to lead to easier and cheaper computations, we chose to replace M by the diagonalized matrix D, obtained by using a quadrature formula which does not deteriorate the accuracy of the method. The problem to solve becomes:

Find E^{n+1} such that

$$\frac{1}{\Delta t^2} D(E^{n+1} - 2E^n + E^{n-1}) + c^2 K E^n = G^n, \tag{2.19}$$

where G^n denotes the right-hand side of (2.18).

To obtain the corresponding finite differences expression, we introduce a 1D regular grid $x_i = (i-1)\Delta x$, $i = 1, 2, ..., m$, so that the exact mass matrix is defined by

$$F^t M E = \int_0^L EF \, dx = \frac{\Delta x}{6} \sum_i F_i(E_{i+1} + 4E_i + E_{i-1}), \tag{2.20}$$

and the approximate diagonal mass matrix is such that

$$F^t D E = \Delta x \sum_i F_i E_i \simeq \int_0^L EF \, dx, \tag{2.21}$$

that is a second-order approximation of (2.20).

Finally the rigidity matrix is given by

$$F^t K E = \int_0^L \nabla E \nabla F \, dx = \frac{1}{\Delta x} \sum_i F_i(-E_{i+1} + 2E_i - E_{i-1}). \tag{2.22}$$

It is easy to check that the left-hand side of (2.19) is the classical finite difference operator given by

$$\frac{E_i^{n+1} - 2E_i^n + E_i^{n-1}}{\Delta t^2} - c^2 \frac{E_{i+1}^n - 2E_i^n + E_{i-1}^n}{\Delta x^2}, \tag{2.23}$$

which is a nondissipative centered second-order scheme, stable under the condition $c\Delta t/\Delta x \leq 1$ in 1D. As is well known, the extension of this discretization to a 2D or 3D regular grid leads to the classical Yee scheme [16], which generates numerical instabilities when dealing with shocks or with stiff sources. Furthermore, various authors [7, 13] have shown that this discretization of the Maxwell equations, coupled with a particular scheme (2.12)–(2.14) for the resolution of the Vlasov equation can cause unphysical effects on the field solution, which may interact with particles to induce rapidly growing numerical instabilities. In order to avoid these numerical instabilities, we introduce a new scheme.

2.2. Construction of the New Scheme

Let us consider the formulation (2.18) with the complete mass matrix M which implies solving the algebraic system

$$ME^{n+1} = M(2E^n - E^{n-1}) + \Delta t^2(F^n - c^2 KE^n). \tag{2.24}$$

We decompose the matrix M into two parts

$$M = (M - D) + D, \tag{2.25}$$

and we keep the diagonalized part D in the left-hand side to avoid the inversion of a full mass matrix, so that (2.24) becomes

$$DE^{n+1} = M(2E^n - E^{n-1}) + \Delta t^2(F^n - c^2 KE^n) - (M - D)E^{n+1}. \tag{2.26}$$

It remains to use a suitable prediction $\overline{E}^{n+1}$ of the right-hand side E^{n+1}, to obtain in all the cases an explicit time-stepping method. We choose

$$\overline{E}^{n+1} = \varepsilon E^n + (1 - \varepsilon)\tilde{E}^{n+1}, \tag{2.27}$$

where ε is a positive parameter ($\varepsilon \geq 0$), and where $\tilde{E}^{n+1}$ is the solution of the problem (2.19), namely

$$\tilde{E}^{n+1} = 2(E^n - E^{n-1}) - \Delta t^2 D^{-1}(F^n - c^2 KE^n). \tag{2.28}$$

Our new scheme can finally be expressed as

$$DE^{n+1} = M(2E^n - E^{n-1}) + \Delta t^2(F^n - c^2 KE^n) - (M - D)(\varepsilon E^n + (1 - \varepsilon)\tilde{E}^{n+1}). \tag{2.29}$$

It has to be pointed out that the expression (2.29) is a finite-element formulation valid either in one, two, or three dimensions. The finite difference form of this scheme is easily derived from (2.29). It will be derived here in one dimension, but

can be easily obtained in a similar way in two and three dimensions. By using the expression (2.28) of $\tilde{E}^{n+1}$ and the integration formulae (2.20)–(2.22), we obtain

$$E_i^{n+1} - \left(\frac{\varepsilon}{6}E_{i+1}^n + \left(2 - \frac{\varepsilon}{3}\right)E_i^n + \frac{\varepsilon}{6}E_{i-1}^n\right) + \left(\frac{\varepsilon}{6}E_{i+1}^{n-1} + \left(1 - \frac{\varepsilon}{3}\right)E_i^{n-1} + \frac{\varepsilon}{6}E_{i-1}^{n-1}\right)$$
$$- \frac{c^2\Delta t^2}{6\,\Delta x^2}[-(1-\varepsilon)E_{i+2}^n + (10-4\varepsilon)E_{i+1}^n - (18-6\varepsilon)E_i^n + (10-4\varepsilon)E_{i-1}^n$$
$$- (1-\varepsilon)E_{i-2}^n] = 0. \tag{2.30}$$

Remarks. 1. The time discretization, for $\varepsilon = 0$, coincides with the leapfrog scheme used in (2.23), whereas the space one is a five-mesh-point discretization. For $\varepsilon = 1$, the space discretization coincides with the space discretization in (2.23), whereas the time one is different; the time values $E(t^{n-1})$ and $E(t^n)$ are split on the three neighbouring nodes x_{i-1}, x_i, x_{i+1} with a coefficient related to ε. The new scheme is, however, explicit for all ε since the time value $E(t^{n+1})$ is never split. In the numerical experiments, it seems natural to choose $\varepsilon \in [0, 1]$.

2. The expression (2.29) allows us to see this scheme as a kind of prediction–correction: (2.28) consists of a prediction that coincides with (2.23) in the finite difference formulation; (2.29) is the correction which is decentered as soon as $\varepsilon \neq 0$. If $\varepsilon = 1$, there is no more prediction and the scheme is decentered at most. We will see more precisely these properties in the next section, especially the role of the parameter ε.

2.3. Elementary Numerical Properties of the New Scheme

In this section, we investigate some elementary properties which are useful for a numerical implementation, namely the consistency, the stability, the dissipation, and the order of the scheme.

Let us call $S_\varepsilon(E_i^n)$ the left-hand side of (2.30); by using Taylor expansions we obtain the approximation:

$$S_\varepsilon(E_i^n) = \left(\frac{\partial^2}{\partial t^2} - c^2\frac{\partial^2}{\partial x^2}\right)E(x_i, t^n) + O(\Delta t^2 + \Delta x^2)$$
$$- \frac{\varepsilon}{6}\left[\frac{\Delta x^2}{\Delta t}\frac{\partial^3}{\partial t \partial x^2}E(x_i, t^n) + O\left(\Delta x^2 + \frac{\Delta x^4}{\Delta t}\right)\right]. \tag{2.31}$$

Remarks. 1. We can deduce from (2.31) that the new scheme is, in 1D, a consistent approximation of the wave operator if and only if $\Delta x^2/\Delta t$ is bounded. This condition is always fulfilled in practice.

2. When $\varepsilon = 0$ this scheme is of order 2 in time and in space.

3. When $\varepsilon \neq 0$ the scheme is of order 1 and the extra term proportional to the third-order derivative, namely $\partial^3 E/\partial t \partial x^2$, can be identified with a viscosity term which induces a certain amount of dissipation, according to the value of ε. This point will be confirmed and specified with the Fourier analysis. In practice, however,

the numerical examples show that the precision is not significantly affected by the loss of the order when dealing with $\varepsilon \neq 0$.

We therefore consider the finite difference expression (2.30) for studying the stability of the scheme by Fourier techniques.

Taking the Fourier transform of (2.30) (with $\beta = c(\Delta t/\Delta x)$, $\alpha = \sin^2(k\ \Delta x/2)$, and $\hat{E}$ the Fourier transform of E), we obtain

$$\hat{E}^{n+1} = \left[2\left(1 - \frac{\varepsilon}{3}\alpha^2\right) - \frac{\beta^2}{3}(12\alpha^2 + 8(1-\varepsilon)\alpha^4)\right]\hat{E}^n - \left(1 - 2\frac{\varepsilon}{3}\alpha^2\right)\hat{E}^{n-1}, \quad (2.32)$$

or equivalently, by introducing the transfer matrix,

$$\begin{pmatrix} \hat{E}^{n+1} \\ \hat{E}^n \end{pmatrix} = \begin{pmatrix} 2\left(1 - \frac{\varepsilon}{3}\alpha^2\right) - 4\frac{\beta^2}{3}\alpha^2(3 + 2(1-\varepsilon)\alpha^2) & -\left(1 - 2\frac{\varepsilon}{3}\alpha^2\right) \\ 1 & 0 \end{pmatrix} \begin{pmatrix} \hat{E}^n \\ \hat{E}^{n-1} \end{pmatrix}. \quad (2.33)$$

The stability is fulfilled when the two eigenvalues λ_1, λ_2 are such that $|\lambda_1| < 1$, $|\lambda_2| < 1$. After some algebra, it can be shown that:

Property 2.1. The scheme is stable if

$$\beta \leq \sqrt{\frac{3-\varepsilon}{5-2\varepsilon}}. \quad (2.34)$$

Note first that, in the case $\varepsilon = 0$, this condition ($\beta < 0.774$) is slightly more restrictive than the leapfrog stability condition ($\beta \leq 1$). The maximum value is, however, rising with ε, becoming less restrictive from $\varepsilon = 0$ to $\varepsilon = 1$ (where $\beta \leq 0.816$).

As a by-product of the stability study, we can evaluate the dissipation of the scheme. For doing this, we have to investigate the positions of the eigenvalues compared with 1. We obtain that $\lambda_1 = \overline{\lambda_2}$ are such that

$$|\lambda_1|^2 = |\lambda_2|^2 = |\lambda|^2 = 1 - 2\frac{\varepsilon}{3}\alpha^2. \quad (2.35)$$

We have, therefore, the following property.

Property 2.2. The scheme is dissipative for $\varepsilon \in]0, 1]$. This dissipation can be evaluated by

$$1 - |\lambda| = 1 - \sqrt{1 - \frac{2}{3}\alpha^2\varepsilon}\,. \quad (2.36)$$

For $\varepsilon = 0$, the scheme is nondissipative.

Remark. Note that this dissipation is independent of β. Moreover, it depends on α in such a way that the higher the frequencies are, the greater the dissipation is. Observe finally that the greater ε is, the more dissipative the scheme is.

3. LINEAR ANALYSIS OF THE WAVES IN A FLUID PLASMA

As we mentioned in the Introduction, we will use in this section a fluid plasma model to describe the motion of the particles. We will assume that all the particles could be considered as a homogeneous field-free cold plasma, drifting with a constant velocity u_0. With these assumptions, we will illustrate in a first part how a Tcherenkov instability could grow in the continuous model. The second part will be devoted to the analysis of the numerical Tcherenkov instability. We will in particular see in which way the new scheme can reduce this instability.

3.1. Stability Analysis in the Continuous Problem

We begin this section by deriving the dispersion relation. We refer the reader to a large bibliography for more details ([17, 6, 7] among others), even if the relativistic case we develop here is not commonly derived.

The fluid equations for the electrons and the ions are written as

$$\begin{aligned} \frac{\partial n_\alpha}{\partial t} + \nabla \cdot (n_\alpha u_\alpha) &= 0 \\ \frac{\partial p_\alpha}{\partial t} + \left(\frac{p_\alpha}{\gamma_\alpha} \cdot \nabla\right) p_\alpha - \frac{q_\alpha}{m_\alpha}\left(E + \frac{p_\alpha}{\gamma_\alpha} \times B\right) &= 0, \end{aligned} \tag{3.1}$$

where n_α and u_α denote the particle density and velocity for each species of particle α, with $p_\alpha = \gamma_\alpha u_\alpha$ and $\gamma_\alpha = (1 + p_\alpha^2/c^2)^{1/2}$. The system (3.1) is coupled with the Maxwell equations (2.3)–(2.6), where, in this context, the right-hand sides J and ρ have to be expressed as a function of n_α and u_α, namely,

$$\begin{aligned} J &= \sum_\alpha q_\alpha n_\alpha u_\alpha, \\ \rho &= \sum_\alpha q_\alpha n_\alpha. \end{aligned} \tag{3.2}$$

The first step consists in linearizing this system around the homogeneous steady-state defined by (α standing for the electrons or the ions)

$$\begin{aligned} u_\alpha &= u_0, \\ n_\alpha &= n_0 = \text{const}, \\ \sum_\alpha q_\alpha &= 0, \end{aligned}$$

so that, in this equilibrium,

$$E_0 = 0, \quad B_0 = 0.$$

By retaining only the first-order terms of the expansion around this steady state for the electrons, we obtain

$$\begin{gathered}
\frac{\partial n_1}{\partial t} + \frac{1}{\gamma_0}(n_0 \nabla \cdot p_1 + p_0 \cdot \nabla n_1) = 0, \\
\frac{\partial p_1}{\partial t} + \left(\frac{p_0}{\gamma_0} \cdot \nabla\right) p_1 - \frac{q}{m}\left(E_1 + \frac{p_0}{\gamma_0} \times B_1\right) = 0, \\
\nabla \cdot E_1 = \frac{1}{\varepsilon_0}(q\, n_1), \\
\nabla \cdot B_1 = 0, \\
\frac{1}{c^2}\frac{\partial E_1}{\partial t} - \nabla \times B_1 = -\mu_0 \frac{q}{\gamma_0}\left(n_0\left(p_1 - \frac{p_0 p_1}{c^2 + p_0^2} p_0\right) + n_1 p_0\right), \\
\frac{\partial B_1}{\partial t} + \nabla \times E_1 = 0,
\end{gathered} \tag{3.3}$$

with $p_0 = \gamma_0 u_0$ and $\gamma_0 = (1 + p_0^2/c^2)^{1/2}$, the index 1 denoting the order of the approximation. A Fourier transform in (x, t) of (3.3) and the elimination of $\hat{B}_1$, $\hat{u}_1$, $\hat{n}_1$ leads to the dispersion relation

$$\begin{aligned}
(\omega^2 - c^2|k|^2)\hat{E}_1 + c^2(k \cdot \hat{E}_1)k = {} & \frac{\omega}{\omega - k \cdot u_0}\frac{\omega_p^2}{\gamma_0}\left(\left(1 - \frac{u_0 \cdot k}{\omega}\right)\hat{E}_1 + \frac{u_0 \cdot \hat{E}_1}{\omega}k\right. \\
& \left. - \frac{p_0}{c^2 + p_0^2}\left(\left(1 - \frac{u_0 \cdot k}{\omega}\right) p_0 \cdot \hat{E}_1 + \frac{u_0 \cdot \hat{E}_1}{\omega} p_0 \cdot k\right)\right) \\
& + \frac{\omega}{(\omega - k \cdot u_0)^2}\frac{\omega_p^2}{\gamma_0}\left(\left(1 - \frac{u_0 \cdot k}{\omega}\right)(\hat{E}_1 \cdot k) + \frac{|k|^2}{\omega}(u_0 \cdot \hat{E}_1)\right) u_0,
\end{aligned} \tag{3.4}$$

where ω_p denotes the plasma frequency defined by $\omega_p^2 = q^2 n/\varepsilon_0 m$.

We introduce now (ξ, η, ζ) a direct orthonormal basis of $\mathbb{R}^3$, such that $\xi = k/|k|$, $u_0 = |u_0|(\cos\theta\xi + \sin\theta\eta)$, $0 \le \theta \le \pi$, and we write the matrix $D(\omega, k)$ such that $D(\omega, k)\,\hat{E}1 = 0$. Some algebra yields

$$D(\omega, k) = \begin{pmatrix} D_{11} & D_{12} & 0 \\ D_{12} & D_{22} & 0 \\ 0 & 0 & D_{33} \end{pmatrix} \tag{3.5}$$

with

$$
\begin{aligned}
D_{11} &= \gamma_0\omega^2 - \frac{\omega_p^2\omega^2}{(\omega - |u_0||k|\cos\theta)^2} + \frac{\omega_p^2\omega\cos^2\theta}{\omega - |u_0||k|\cos\theta}\frac{p_0^2}{p_0^2 + c^2},\\
D_{12} &= -\frac{\omega_p^2\omega|u_0||k|\sin\theta}{(\omega - |u_0||k|\cos\theta)^2} + \frac{\omega_p^2\omega\sin\theta\cos\theta}{\omega - |u_0||k|\cos\theta}\frac{p_0^2}{p_0^2 + c^2},\\
D_{22} &= \gamma_0(\omega^2 - c^2|k|^2) - \frac{\omega_p^2(\omega^2 - 2\omega|u_0||k|\cos\theta + |u_0|^2|k|^2)}{(\omega - |u_0||k|\cos\theta)^2}\\
&\quad + \frac{\omega_p^2\omega\sin^2\theta}{\omega - |u_0||k|\cos\theta}\frac{p_0^2}{p_0^2 + c^2},\\
D_{33} &= \gamma_0(\omega^2 - c^2|k|^2) - \omega_p^2,
\end{aligned}
\tag{3.6}
$$

so that the dispersion relation (3.4) can be rewritten

$$
\det D(\omega, k) = (\gamma_0(\omega^2 - c^2|k|^2) - \omega_p^2)\,\Delta(\omega, k) = 0, \tag{3.7}
$$

where $\Delta(\omega, k)$ is the determinant of the two first columns and rows of $D(\omega, k)$. The solutions $\omega(k)$ of $\gamma_0(\omega^2 - c^2|k|^2) - \omega_p^2 = 0$ correspond to electromagnetic waves. The interesting point consists in finding the roots of $\Delta(\omega, k)$, that is, without any assumption, a polynomial of degree 6. If we first consider the case $\theta = 0$, that means u_0 parallel to k, $\Delta(\omega, k)$ is a polynomial of degree 3 in ω. This polynomial can be written in the canonical form $\omega^3 + p\omega + q$. It can be then verified that the condition $4p^3 + 27q^2 \leq 0$ is always fulfilled, so that the roots of $\Delta(\omega, k)$ are always real and the system is stable. Let us consider now the case $\theta = \pi/2$, which corresponds to a velocity u_0 perpendicular to k. We obtain for $\Delta(\omega, k)$ a polynomial of degree 2 in ω^2, the solutions of which are

$$
\begin{aligned}
\omega_\pm^2 = \frac{1}{2\gamma_0}\Bigg(&\omega_p^2\left(2 - \frac{p_0^2}{p_0^2 + c^2}\right) + c^2|k|^2\\
&\pm \sqrt{\left(c^2|k|^2 - \omega_p^2\frac{p_0^2}{p_0^2 + c^2}\right) + 4\omega_p^2|k|^2(c^2 - \gamma_0(c^2 - |u_0|^2))}\Bigg)
\end{aligned}
\tag{3.8}
$$

and are positive under the condition

$$
\omega_p^4\left(1 - \frac{p_0^2}{p_0^2 + c^2}\right) + \gamma_0\omega_p^2|k|^2(c^2 - |u_0|^2) > 0. \tag{3.9}
$$

This condition is obviously fulfilled in the continuous problem we considered, $|u_0|$ being always less than c with our assumptions (propagation in the vacuum, etc.).

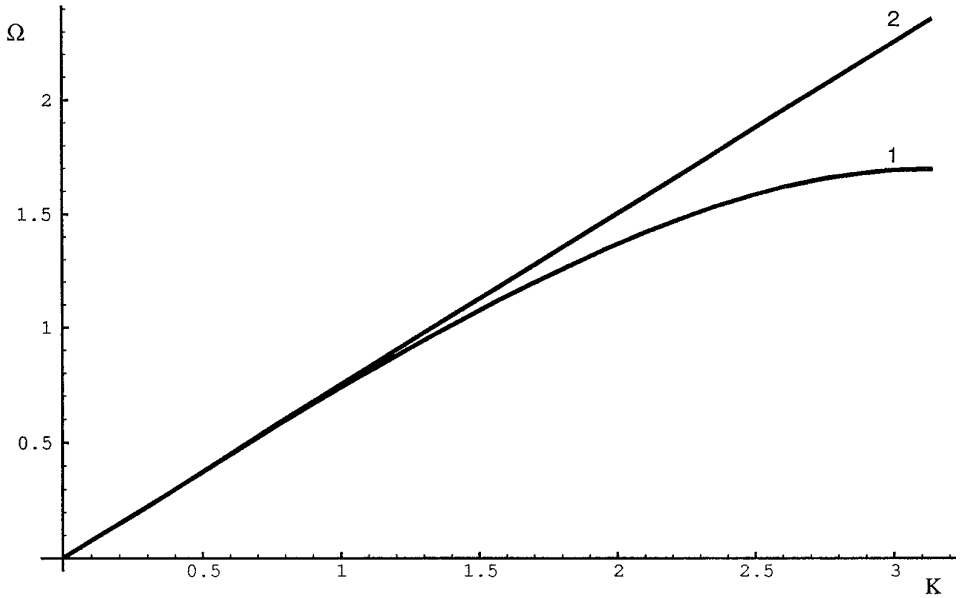

FIG. 1. Dispersion relation for the leapfrog scheme[1] and the continuous case[2].

Consider now a medium in which $|u_0|$ can be greater than c. We can then determine a limit wavenumber k_{lim} defined by

$$k_{\text{lim}}^2 = \frac{\omega_p^2}{\gamma_0^3(|u_0|^2 - c^2)}, \tag{3.10}$$

such that, for $|k| > k_{\text{lim}}$, the $\omega_-^2(k)$ root of (3.8) is negative. In these conditions, two solutions of the dispersion relation (3.7) are complex (purely imaginary), namely $\pm i\sqrt{|\omega_-^2(k)|}$, that leads to an unwanted exponentially growing wave, which can be identified with a Tcherenkov radiation [17]. Under this condition, the instability will be generated for the wavenumbers k that are greater than the k_{lim} defined in (3.10). This value k_{lim} increases with the plasma frequency ω_p and decreases with the distance from $|u_0|$ to c. In order to understand the numerical Tcherenkov instability, we will extend now this analysis to the discretized problem.

3.2. Numerical Tcherenkov Instability

In the continuous case, the waves propagate at a velocity $c = \omega/k$. After discretization, the waves propagate at a velocity v_ϕ, the phase velocity, that is nothing but a numerical approximation of c. v_ϕ is also expressed as $v_\phi = \omega/k$, but ω and k are in this case related by the relation (3.8). For the leapfrog scheme for instance, the result is well known and the relation reads

$$\frac{\sin^2(\omega\,\Delta t/2)}{(\Delta t/2)^2} = c^2\,\frac{\sin^2(k\,\Delta x/2)}{(\Delta x/2)^2}. \tag{3.11}$$

By introducing the usual dimensionless quantities $\Omega = \omega\,\Delta t$, $K = k\,\Delta x$, $\beta = c(\Delta t/\Delta x)$, and $U_0 = u_0/c$, (3.11) can be written as

$$\sin^2(\Omega/2) - \beta^2 \sin^2(K/2) = 0, \tag{3.12}$$

and for the continuous case, the dispersion relation is

$$\Omega = \beta K.$$

Figure 1 shows the curves $\Omega(K)$ of these relations with $\beta = 0.75$. With the dimensionless variables, we have $v_\phi = c\Omega/\beta K$. As one can see, the leapfrog phase velocity v_ϕ remains always less than c, the difference between v_ϕ and c increasing with the wavenumber k. In these conditions, the particle velocity $|u_0|$ can exceed v_ϕ, especially for the high wavenumbers and if the particles move fast enough. This

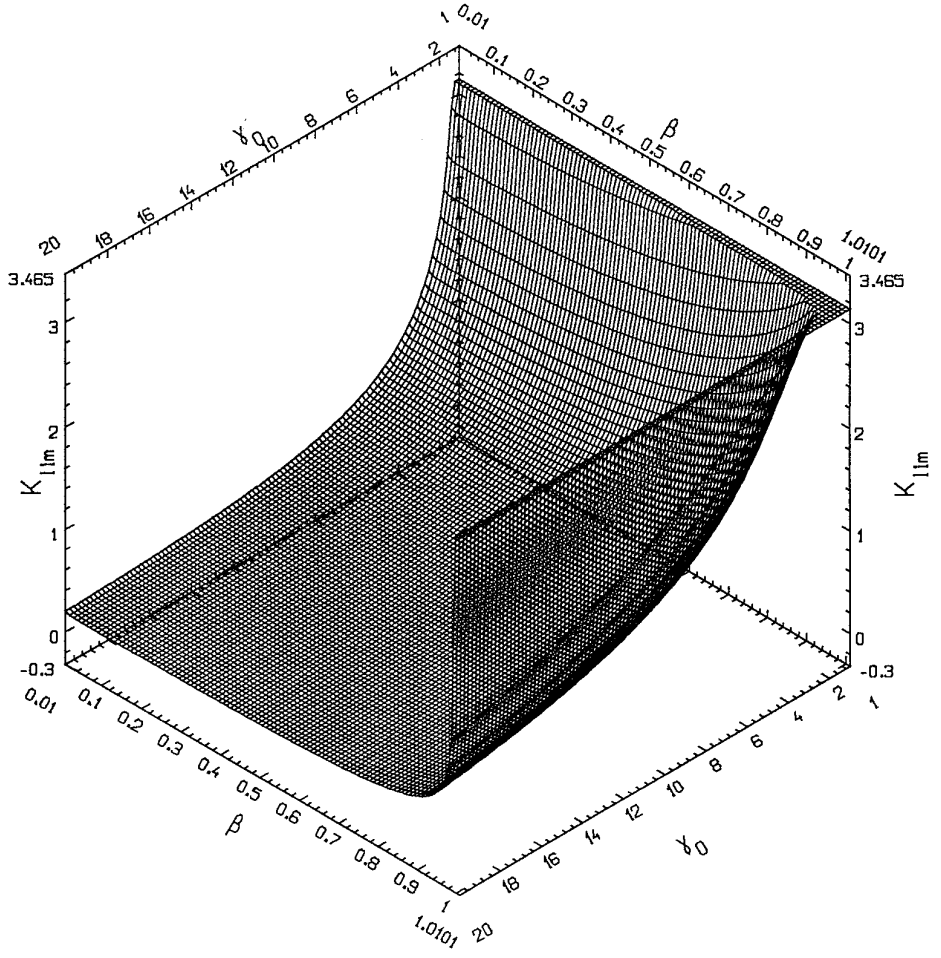

FIG. 2. Stability limit for the leapfrog scheme.

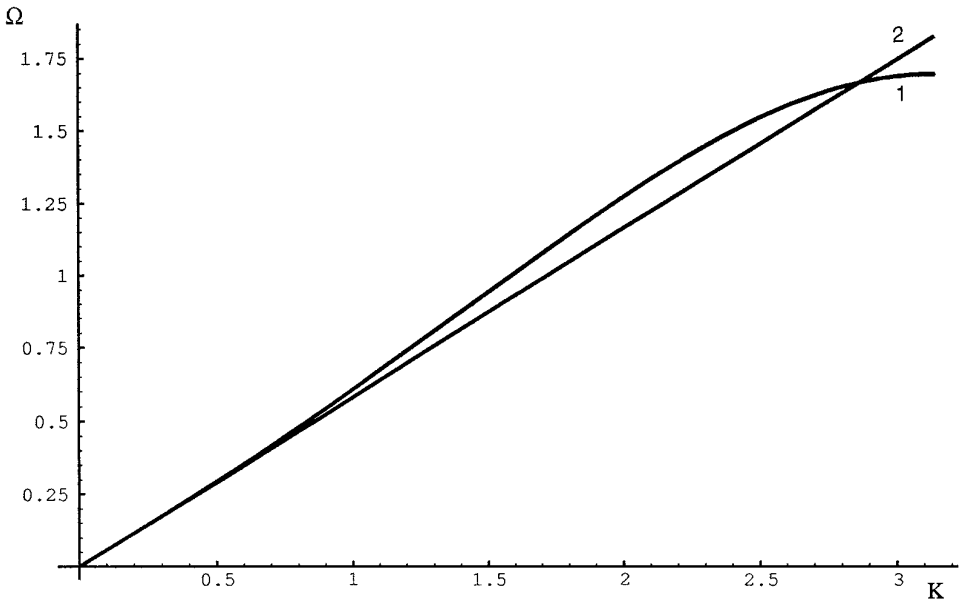

FIG. 3. Dispersion relations for the new scheme[1] and the continuous case[2].

leads to an unwanted exponentially growing instability which is called, by analogy with the continuous case, the numerical Tcherenkov instability.

In order to quantify this phenomenon, we return to the condition (3.9), where c is replaced by the numerical phase velocity ω/k. By doing this, we assume that the errors due to the discretization on the electromagnetic fields and the coupling are negligible. In other terms, it is assumed that the nonpositivity of the roots arising from the term $c - u_0$, is essentially (i.e., at first order) due to the error made on the approximation of the propagation velocity c. For the leapfrog scheme, (3.9) is then approximated, in dimensionless quantities by

$$\frac{\Omega_p^2}{\gamma_0^3} + (2 \arcsin(\beta \sin K/2))^2 - \beta^2 K^2 U_0^2 > 0. \tag{3.13}$$

From this inequality we are not able to guess an analytic expression of $k_{\lim}$, whereas it was possible from (3.10). We then perform a numerical study of (3.13) for different values of Ω_p, with $1 \leq \gamma_0 \leq 20$, $0 < \beta < 1$, and $0 \leq K \leq \pi$. By doing this, we numerically determine that there exists a $K_{\lim}$ such that the inequality (3.13) is fulfilled if and only if $K < K_{\lim}$.

Figure 2 shows $K_{\lim}$ as a function of (β, γ_0), with $\Omega_p \simeq 5.10^{-3}$, which corresponds to typical densities and timesteps of a weakly dense electron beam modelling. On this figure, the value of $K_{\lim}$ is truncated at π corresponding to the two points per wavelength limit value of discretization. One can conclude that there is a large domain in (β, γ_0, K), where the numerical Tcherenkov instability can be produced by the leapfrog scheme.

To overcome this difficulty, the use of high-order discretization methods or finer resolutions are partial remedies, but they do not allow to control the arising of the instabilities. Another approach is to construct numerical schemes whose phase velocities are always greater than c. The new scheme we presented in (2.2) is a first attempt to satisfy this constraint. For $\varepsilon = 0$, the dispersion relations of the new scheme in dimensionless variables is written as

$$\sin^2(\Omega/2) - \frac{\beta^2}{12}(\cos 2K - 10\cos K + 9) = 0. \tag{3.14}$$

This relation is depicted on Fig. 3 with $\beta = 0.75\beta_{\max}$, where $\beta_{\max}$ denotes the admissible maximal value of β such that the stability condition is verified (see (2.34)). In these conditions, this figure is comparable to Fig. 1, obtained with the

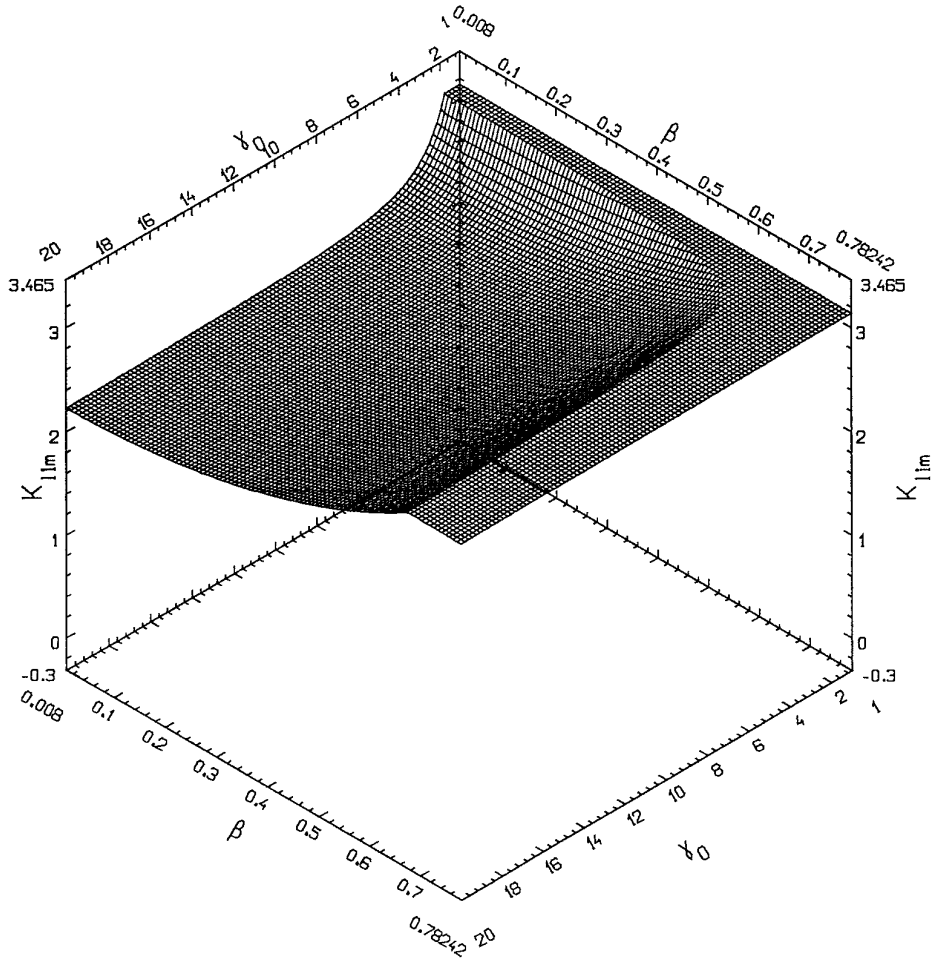

FIG. 4. Stability limit for the new scheme.

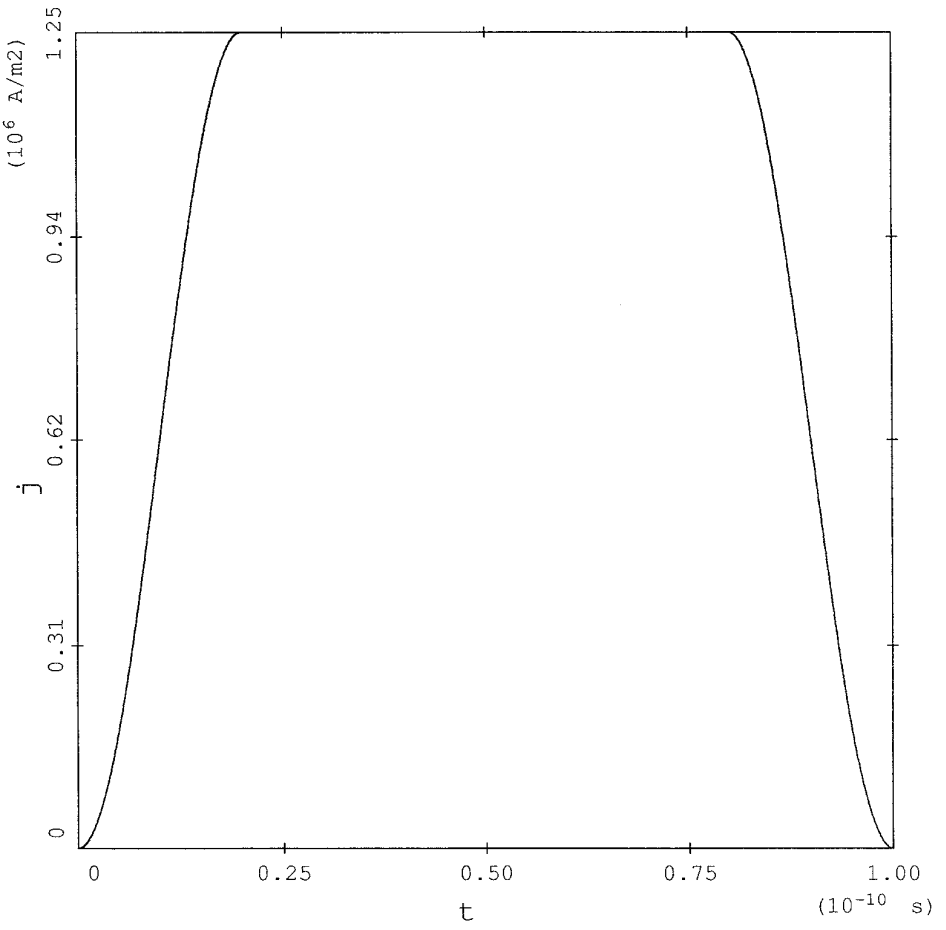

FIG. 5. Time variation of the emission law at the cathode for $\tau = 0.2T$.

leapfrog scheme. One can see that the phase velocity of the new scheme, for this β, is such that

$$v_\phi > c \quad \text{for } K < 2.85,$$
$$v_\phi < c \quad \text{for } K > 2.85,$$

and conclude that the numerical Tcherenkov instability could occur just for the very high wavenumbers. To make this point more precise, one can derive for the new scheme a condition similar to (3.13), saying

$$\frac{\Omega_p^2}{\gamma_0^3} + \left(2 \arcsin\left(\beta \frac{\cos 2K - 10 \cos K + 9}{12}\right)^{1/2}\right)^2 - \beta^2 K^2 U_0^2 > 0. \qquad (3.15)$$

As for the leapfrog case, it can be numerically shown that there exists a K_{lim}, such that the inequality (3.15) is fulfilled if and only if $K < K_{\text{lim}}$. Figure 4 shows

K_{lim} as a function of (β, γ_0), in the same conditions as for the leapfrog scheme (see Fig. 2). The stability domain here is obviously larger than in the first case. Then we may expect the numerical Tcherenkov instability to occur for a small number of wavelengths. In the following section, we will see how to reduce these remaining instabilities again with the aid of the dissipation term ($\varepsilon \neq 0$) in the new scheme.

4. NUMERICAL RESULTS

The stability analysis was developed by assuming a homogeneous neutral plasma. The numerical application we present here is, however, concerning a stiff short electron bunch. Consider a two-dimensional device in axisymmetric geometry (r, z). An electron bunch is emitted from a cathode at the input $z = 0$. It is accelerated by an external electric field and confined by a longitudinal B_z magnetic field. We follow the motion of these particles in a 50-cm drift tube. The electron

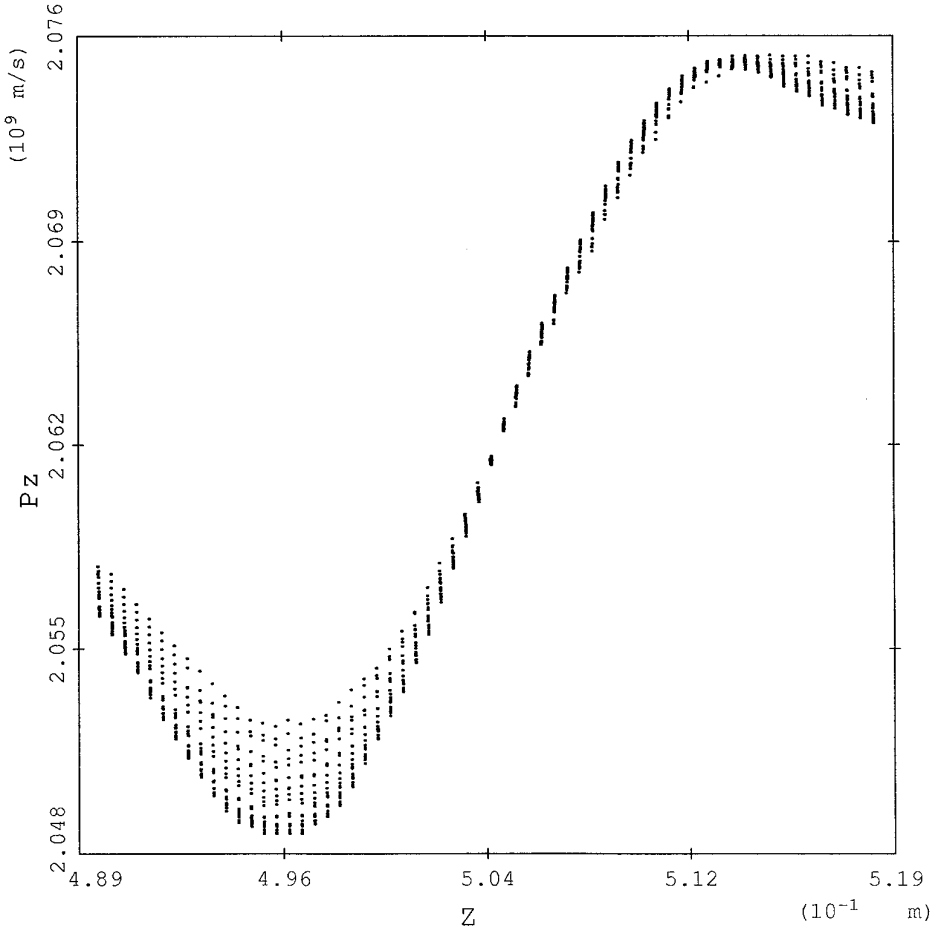

FIG. 6. Phase space for a smooth beam (leapfrog and new scheme).

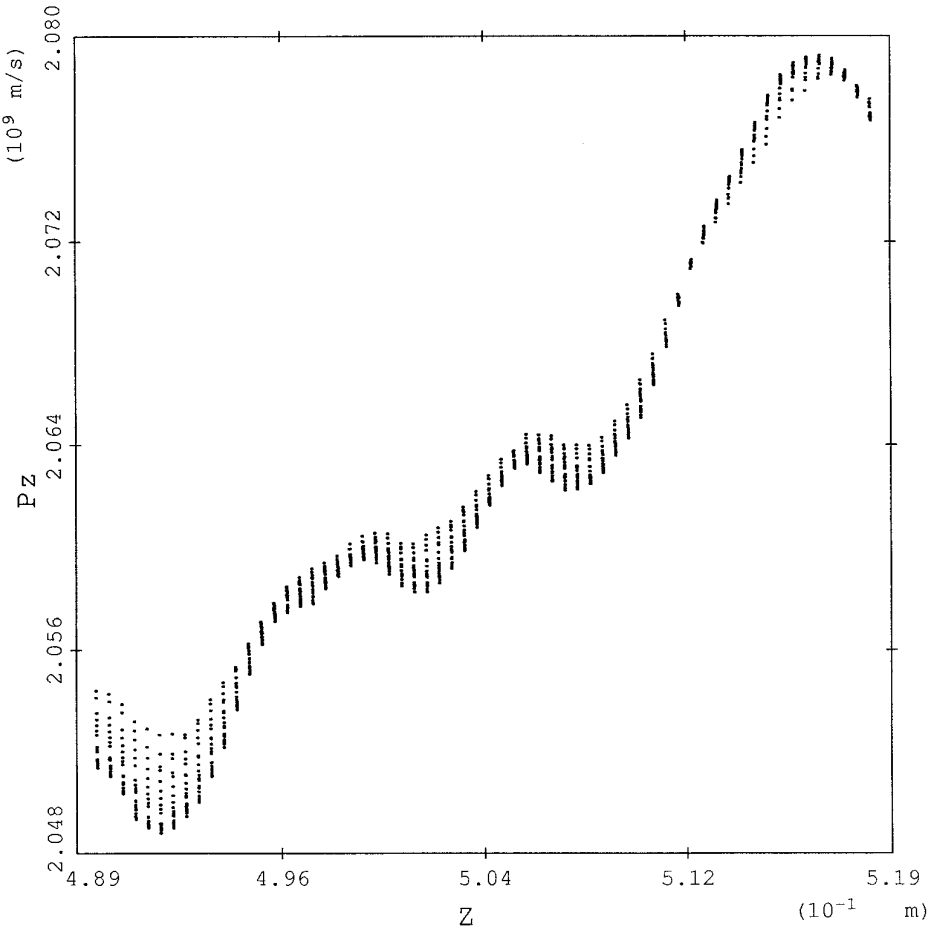

FIG. 7. Phase space for a stiff beam (leapfrog).

bunch dynamics is hardly dependent on the time and axial (r) variations of the emission law of the cathode current. We choose here:

if $r \leq R$,

$$j(r,t) = \frac{Q}{2S(T-\tau)}\left[1 + \sin\left(\frac{\pi}{\tau}(t - \tau/2)\right)\right], \qquad 0 \leq t \leq \tau,$$

$$j(r,t) = \frac{Q}{S(T-\tau)}, \qquad \tau \leq t \leq T - \tau,$$

$$j(r,t) = \frac{Q}{2S(T-\tau)}\left[1 + \cos\left(\frac{\pi}{\tau}(T - \tau - t)\right)\right], \quad T - \tau \leq t \leq T,$$

$$j(r,t) = 0, \qquad t > \tau;$$

if $r > R$, $j(r, t) = 0$,

where Q denotes the total charge of the beam, S is the area of the emission surface (a circle with a radius R), T is the emission duration, and τ characterizes the longitudinal stiffness of the bunch.

The emission law time variation is depicted Fig. 5 with $T = 100\ ps$, $\tau = 20\ ps$, $Q = 10\ nc$, $S = 1\ cm^2$. As we previously mentioned, the numerical simulation of sufficiently stiff bunches with classical schemes (as the leapfrog) leads to instabilities.

In order to investigate this phenomenon, the results obtained with the new scheme and the leapfrog scheme will be compared. In this context, the most useful diagnostic is the phase space representation z/P_z, where P_z denotes here the "normalized momentum," i.e. $P_z = \gamma V_z$. It will be shown after 50 cm of transport, where γ_0 is then equal to 7. The computational domain is regularly discretized with square meshes divided into two triangles, in order to be in a situation quite similar to finite differences. We define a pseudo space step Δx equal to the length of the cell sides.

As a first case, we choose $\tau = T/2$ to obtain a beam which is smooth in the longitudinal direction. The parameters are $\Delta x = 7 \times 10^{-4} m$ and $\Delta t = 1.6 \times 10^{-12}$, leading to $\beta \simeq 0.68$. Figure 6 shows the phase space z/P_z obtained with the leapfrog

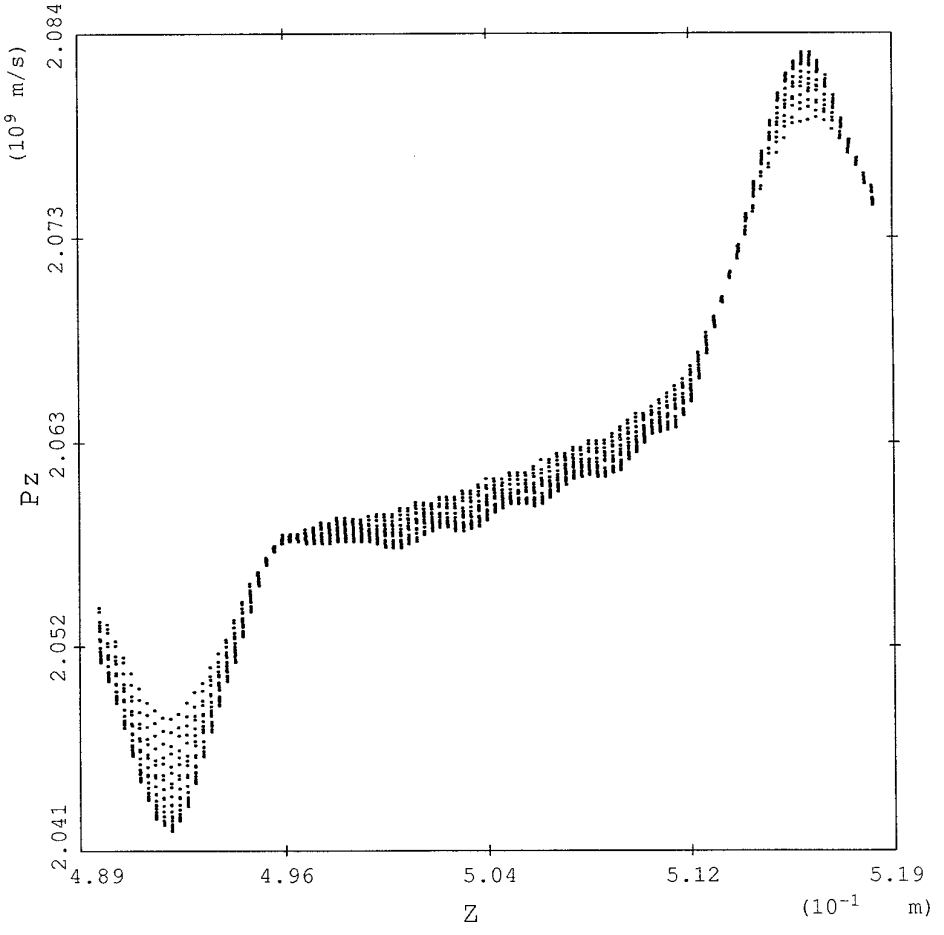

FIG. 8. Phase space for a stiff beam (new scheme, $\varepsilon = 0$).

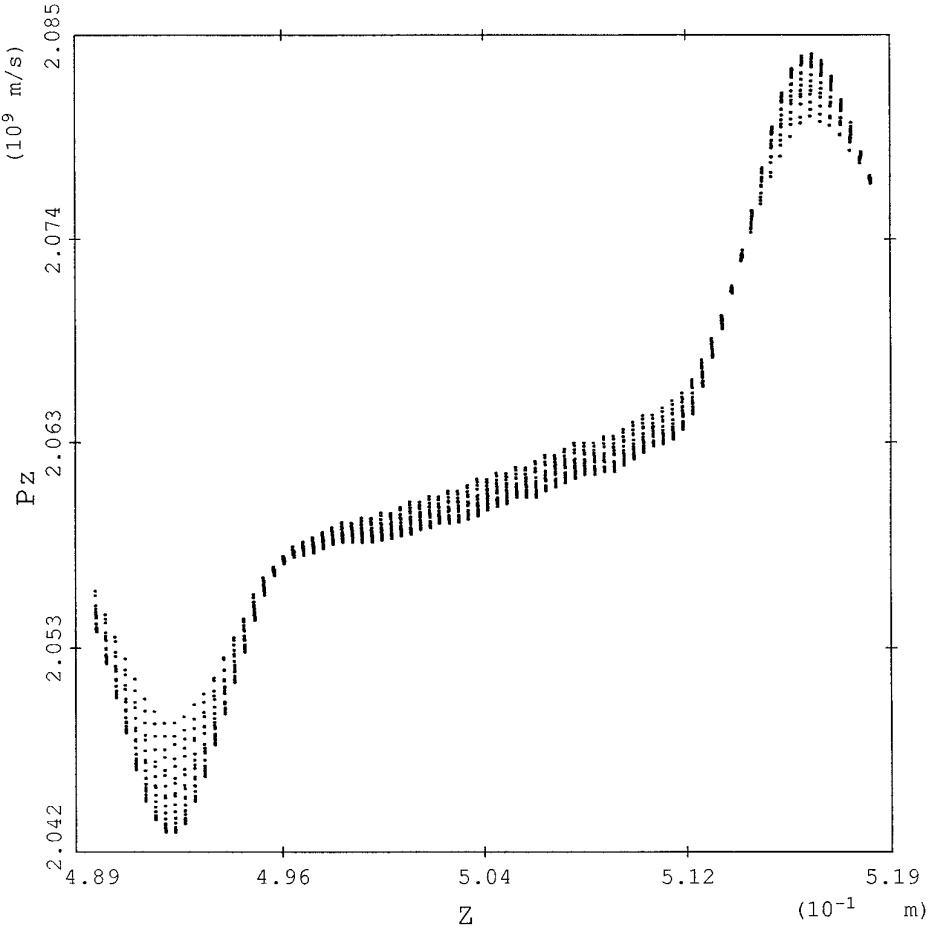

FIG. 9. Phase space for a stiff beam (new scheme, $\varepsilon = 0.1$).

scheme; no instability can be observed. The same case performed with the new scheme and $\varepsilon = 0$ give exactly the same result.

Consider now the case where $\tau = 0.2\ T$ (see Fig. 5). Figure 7 shows the result obtained with the leapfrog scheme. One can see the appearance of the early stage of an unphysical high amplitude oscillation that would continue to grow up if we let the simulation go on. Also it has to be pointed out that the energy variations at the beam head and tail are due to the axial self-electric field (i.e. are *not* an instability). One can measure the wavelength of this oscillation; we obtain $\lambda \simeq 5.7 \times 10^{-3}$ that corresponds to $K \simeq 0.77$. From (3.13), one can numerically evaluate the wavenumber limit K_{lim}, with the corresponding plasma frequency $\Omega_p = 7.36 \times 10^{-3}$. We obtain $K_{\text{lim}} = 0.67$, that is consistent with the previous result.

The same computation is then performed with the new scheme and $\varepsilon = 0$ in analogous conditions, namely $\Delta t = 1.23 \times 10^{-12} s$ ($\beta \simeq 0.53$, i.e., $\simeq 0.68\ \beta_{\max}$). The phase space z/P_z, depicted in Fig. 8 still shows an unwanted instability, but its amplitude is strongly damped and its wavelength is shorter than in the leapfrog

case. The corresponding K is about $K \simeq 1.78$ and the wavenumber limit obtained from (3.15), with $\Omega_p = 5.27 \times 10^{-3}$ is $K_{\lim} = 2.80$.

Under these conditions, the stability analysis developed in Section 3 leads us to predict that the wavenumber of the Tcherenkov instability occurring with the new scheme is higher than the one occurring with the leapfrog scheme. However, it does not allow us to predict precisely a $K_{\lim}$ compatible with the numerical results, even if it proved to be qualitatively correct. This gap can be explained by recalling first that the stability analysis was developed with a neutral homogeneous plasma, whereas the previous example is concerned with an electron bunch. Then, it was used as finite differences discretisation of the Maxwell equations, whereas a finite element method on triangles is used in practice.

In order to reduce the remaining instability, we use the property that the new scheme induces dissipation for $\varepsilon \neq 0$. As we previously mentioned, this dissipation increases with the frequency, which is well adapted here. One can see on Fig. 9 that the oscillations have practically disappeared from the phase space z/P_z obtained with $\varepsilon = 0.1$, without any other modification of the result. Moreover, the loss on the total energy of the beam is only 2×10^{-4} (in relative value), after a propagation of 50 cm.

5. CONCLUSION

In this paper, we proposed a new scheme for the wave equation, in which the numerical phase velocity is greater than the light velocity in a large domain of the (β, K) space. This property allows us to significantly reduce the numerical Tcherenkov instability that often appears in the Maxwell–Vlasov simulations. By using an additive dissipation term, controlled by a parameter ε, we can improve again this result.

In numerical experiments, we use the finite element version of this scheme to model the motion of particle bunches (see [18]). It could be interesting to apply it in a finite differences code, in order to quantify the performance of this scheme in this context. Finally, we project using this scheme in full plasma simulations.

REFERENCES

1. A. B. Langdon, *J. Comput. Phys.* **6,** 247 (1970).
2. B. B. Godfrey and A. B. Langdon, *J. Comput. Phys.* **20,** 251 (1976).
3. P. W. Rambo and J. Denavit, *J. Appl. Phys.* **64**(2), 474 (1988).
4. E. L. Lindman, *J. Comput. Phys.* **5,** 13 (1970).
5. H. Hokuda, *J. Comput. Phys.* **10,** 475 (1972).
6. R. W. Hockney and J. W. Eastwood, *Computer Simulation Using Particles* (McGraw–Hill, New York, 1981).
7. C. K. Birsdall and A. B. Langdon, *Plasma Physics via Computer Simulation* (McGraw-Hill, New York, 1985).
8. B. B. Godfrey, *J. Comput. Phys.* **15,** 504 (1974).
9. A. Sei and W. W. Symes, *J. Sci. Comput.* **10,** 1 (1995).
10. M. Chapman and E. M. Waisman, *J. Comput. Phys.* **58,** 44 (1985).

11. P. W. Rambo, J. J. Ambrosiano, A. Friedman, and D. E. Nielsen Jr., in *Proceedings 13th Conf. Numer. Simul. of Plasmas, Santa Fe, NM,* 1989.
12. A. Friedman, *J. Comput. Phys.* **90,** 292 (1990).
13. A. Friedman, J. J. Ambrosiano, J. K. Boyd, S. T. Brandon, D. E. Nielsen, Jr. and P. W. Rambo, in *Proceedings US-Japan Workshop on Advanced Comp. Simul. Tech. Appl. Plas. and Fus., L.A., Cal.,* (1990).
14. F. Assous, P. Degond, E. Heintze, P. A. Raviart and J. Segré, On a finite-element method for solving the three-dimensional Maxwell equations, *J. Comput. Phys.* **109,** 222 (1993).
15. F. Assous, P. Degond, and J. Segré, A particle-tracking method for the 3D electromagnetic PIC codes on unstructured meshes, *Comput. Phys. Commun.* **72,** 105 (1992).
16. K. S. Yee, *IEEE Trans. Antennas Propag.* **14,** 302 (1966).
17. N. A. Krall and A. W. Trivelpiece, *Principles of Plasma Physics* (McGraw-Hill, New York, 1973).
18. A. Adolf, F. Assous, E. Piault, and J. Segré, M3V: A multi-purpose 3D code for microwave modelling in arbitrary geometry, *IEEE Trans. MTT,* submitted.